RESEARCH PAPER

Microstructure, mechanical properties, and corrosion resistance of friction stir welded Mg-Al-Zn alloy thick plate joints

Fenjun Liu [1,2] · Jianbo Liu [1,2] · Yan Ji [1,2] · Yanxia Bai [1]

Abstract

Mg-Al-Zn (AZ31) of 10-mm thick plates were subjected to friction stir welding (FSW) using a conventional tool (CT) and bobbin tool (BT), respectively. The microstructure, room temperature tensile properties, dynamic compressive mechanical properties, and corrosion resistance of the base metal (BM) and various regions of the friction stir welded joints were investigated systematically. The mean grain size, dislocation density, and precipitate distribution in the various regions of the friction stir welded joints were various due to different thermal cycle and plastic deformation. Compared with the CT, a relatively more homogeneous microstructure, a larger number of high-density dislocations and precipitates were produced in the various regions of the joint prepared by the BT due to higher thermal cycle and strain rate. As a result, the friction stir welded joint prepared by the BT exhibits excellent tensile properties and dynamic compressive mechanical properties, and outstanding corrosion resistances compared to those of the CT. In addition to slight changes in tensile properties and dynamic compressive mechanical properties, the corrosion resistance of the joint prepared by the BT was significantly improved compared to the BM. FSW with BT was suggested to be the optimal method to weld AZ31 alloy thick plate.

Keywords AZ31 alloy · Microstructure · Tensile properties · Dynamic compressive mechanical properties · Corrosion resistance · Thick plate

1 Introduction

In addition to being known as a green engineering materials, magnesium alloys are also considered to be one of the most potential candidates to replace aluminum alloys in some mechanical and structural parts in the applications of aerospace and transportation for achieving lightweight design due to their low density [1–3]. In order to meet cost savings and widen application fields, a reliable welding process of magnesium alloys is inevitable. Magnesium alloys can be welded in a variety of processes, but welding magnesium alloys using conventional fusion process still faces many challenges such as evaporative loss of the alloying elements, hot crack, porosity, and high residual stress [4, 5].

Friction stir welding (FSW) is an innovative solid-state joining process, which can effectively alleviate the disadvantages of conventional fusion welding processes. FSW is considered by designers to be the most suitable for welding non-ferrous metals such as magnesium alloys, aluminum alloys, and copper alloys [6–8]. Moreover, FSW has been successfully used in welding Mg-Al-Zn magnesium alloys [9, 10]. Researchers have conducted a lot of investigations on the microstructure [11], tensile properties [12], and corrosion performances [13] of friction stir welded magnesium alloy joints prepared using a conventional tool (CT). Suhuddin et al. [14] found that the grain structure evolution mainly depended on the texture evolution during FSW of a 2-mm thick AZ31 alloy, and was also affected by the strain geometry effect and discontinuous recrystallization. Chowdhury et al. [15] found in the FSW research of a 2-mm thick AZ31 alloy that the twinned and deformed grains of the as-received base metal (BM) were transformed into equiaxed recrystallized grains

---

✉ Fenjun Liu
   lfjxcmg@126.com

1   College of Energy Engineering, Yulin University, Yulin 719000, China

2   Yulin Key Laboratory of Metal Matrix Composites and Remanufacturing Technology, Yulin University, Yulin 719000, China

after FSW, and the grain size decreased with increasing the welding speed and decreasing the rotation speed. Wang et al. [16] investigated the influence of rotation speed on the room temperature tensile properties of an 8-mm thick friction stir welded AZ31 alloy joint and found that the joint efficiency increased from 71.5 to 90.2% with increasing the rotation speed from 800 to 1200 rpm. By further increasing the rotation speed to 1600 rpm, the joint efficiency was reduced to 78.3%. In addition to the rotation speed and welding speed, Ugender et al. [17] also investigated the influence of tool pin profile on the mechanical properties of a 5-mm thick friction stir welded AZ31 alloy joint and found that the main factors affecting the mechanical properties were rotation speed and welding speed, followed by the tool pin profile. In addition to paying attentions to the influences of conventional process parameters, some researchers have tried to improve the mechanical properties of friction stir welded AZ31 alloy joint by post-weld treatment, changing cooling conditions, and adding nanoparticles. Liu et al. [18] investigated the effect of post-weld hot rolling on the mechanical properties of a 7-mm thick friction stir welded AZ31 alloy joint and found that the joint efficiency increased due to the decrease of microstructure difference between the adjacent regions caused by increasing the rolling reduction. Darras et al. [19] demonstrated that the elongation of the submerged friction stir processed AZ31 alloy was significantly enhanced due to the grain refinement caused by increasing the cooling speed. Rouhi et al. [20] investigated the effects of air cooling and water cooling on the mechanical properties of an 8 thick friction stir welded AZ91 alloy joint and found that the tensile strength of the friction stir welded joint prepared with water cooling was significantly enhanced compared to that of the air cooling.

With the development of FSW of Mg-Al-Zn alloy, some researchers have begun to pay attention to the corrosion resistance of the friction stir welded joint and welding technology of self-reacting FSW with a bobbin tool (BT). Shen et al. [21] demonstrated that the friction stir welded AZ31 alloy joint exhibited a better corrosion resistance in the alkaline solution than in the acidic solution. Abbasi et al. [22] investigated the corrosion resistance of a 6-mm thick friction stir welded zone of AZ31 alloy by incorporation of SiC particles and found that the reinforced friction stir welded zone exhibited excellent corrosion resistance due to formation of oxide film and removal of the local cell. Sahu et al. [23] explored the FSW process of a 4-mm thick AZ31 alloy using a BT and demonstrated that the FSW of AZ31 alloy using a BT with inert medium was an effective solution to enhance the mechanical properties of the joint. The grain size in the NZ is about 12 μm, which is 17.6% of the BM. The maximum tensile strength of the friction stir welded joint prepared using a BT with inert medium is 204.08 MPa, which is 85% of the BM [23]. Up to now, the researches on the FSW of Mg-Al-Zn alloys mainly focus on the thickness between 2 and 8 mm

[8]. However, there are few reports on the FSW of 10-mm thick plate Mg-Al-Zn alloy, especially FSW using a BT. In addition, there are also few reports on the corrosion resistance and dynamic compressive mechanical properties of various regions of the friction stir welded Mg-Al-Zn alloy thick plate joint.

In the current work, the main objective was expected to provide an alternative process for enhancing the mechanical properties and corrosion resistance of the friction stir welded AZ31 alloy thick plate joint. Thus, a thorough analysis was performed on microstructure features, microhardness distributions, room temperature tensile properties, room temperature dynamic compressive mechanical properties, corrosion resistance, and corrosion damage of the various regions in the sound friction stir welded AZ31 alloy thick plate joint.

## 2 Experimental procedures

2.1 Material and FSW

The BM for FSW using a CT and BT was 10-mm thick hot squeezed AZ31 alloy (3Al-1Zn-Mg Bal. wt%) plates with dimensions of 150 mm × 100 mm. Prior to FSW, the edges of the AZ31 alloy thick plates to be welded were mechanically ground using waterproof 1000- to 2000-grit SiC abrasive papers and then cleaned with acetone and ethanol in turn.

A single-pass friction stir butt welding was carried out using a two-dimensional FSW machine (FSW-TS-F08-DZ) with a CT and BT, respectively. Both of the CT and BT were made of H13 die steel. The CT was composed of a concentric rings shoulder with a diameter of 24 mm and a conical pin with the size of 10 mm in average diameter and 9.8 mm in length. The FSW with the CT was performed at the rotation speed of 1200 rpm and welding speed of 200 mm/min with the title angle of 3°. The BT with an upper and lower shoulder diameter of 28 mm and a cylindrical pin with a diameter of 10 mm and length of 9.5 mm were used in the present work. In addition, there are concentric rings on the surface of the upper and lower shoulder, and clockwise threads on the surface of the cylindrical pin. The FSW with the BT was carried out at the rotation speed of 200 rpm and welding speed of 100 mm/min with the title angle of 0°. The processing parameters used in the present work were optimized through a large number of experiments, which can achieve the defect-free FSW of the AZ31 alloy thick plates.

2.2 Microanalysis

Specimens for microstructure observations were taken along the horizontal centerline of the cross section of the friction stir welded joints, as shown in Fig. 1. A standard metallographic method was introduced to polish the specimens with

Fig. 1 Schematic diagram of sampling positions and measured specimens
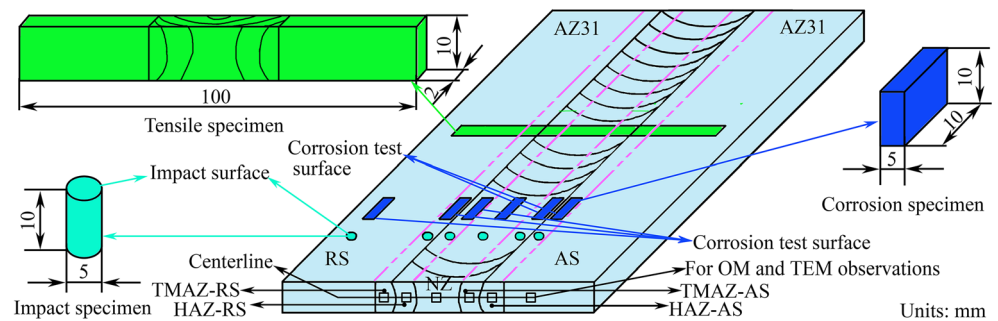
waterproof 1000- to 3000-grit SiC abrasive papers. Fine polishing was performed to prepare a mirror surface using a diamond abrasive paste with the particle size of 1.5 μm. A reagent consisting of 1-g $H_2C_2O_4$ and 1-ml HNO_3 in 150-ml H_2O was applied to reveal the microstructure. The microstructure characteristics were recorded using an optical microscope (OM, OLYMPUS PMG3) and a transmission electron microscope (TEM, FEI TECANI-F30).

2.3 Mechanical and corrosion properties tests

The microhardness, tensile properties, dynamic compressive mechanical properties, potentiodynamic polarization curves, and Nyquist spectras were used to assess the mechanical properties and corrosion resistance of the NZ, the thermal mechanical affected zone (TMAZ), and the heat-affected zone (HAZ) in the friction stir welded joints. The microhardness distributions were recorded using a microhardness tester (HMV-1) along the centerline of the cross section of the joints. Steps, loads, and dwell times for microhardness testing were 0.5 mm, 0.98 N, and 10 s, respectively. The tensile properties of the joints were tested using an electronic universal testing machine (INSTRON 3382) at a crosshead speed of 1 mm/min. The room temperature dynamic compressive mechanical properties were carried out using a split Hopkinson pressure bar at a strain rate of $\sim 1 \times 10^3$ s^{-1}. The potentiodynamic

polarization curves and Nyquist spectras were recorded using a standard three-electrode electrode electrochemical test system (VERSASTAT 400) at a scan rate of 50 mV/s. The corrosion test surface was the side close to the center of the NZ. The tensile fracture surfaces and corrosion damage surfaces were observed using a scanning electron microscope (SEM, TESCAN MIRA3 XMU). The specific sampling positions and measured specimens are shown in Fig. 1.

3 Results and discussions

3.1 Microstructure evolution

The surface morphologies of the friction stir welded joints produced using the CT and BT are presented in Fig. 2. Welding defects such as grooves and voids are not observed on the surface appearances of the joints, indicating that sound friction stir welded AZ31 alloy thick plate joints prepared using the CT and BT under the investigated welding parameters. However, a large flash is observed on the surface of the joint prepared using the BT, which is mainly due to the poor rigid clamping of the BT and workpieces during FSW. As a result, the effective thickness of the NZ is significantly reduced.

Fig. 2 Top surface morphologies of the friction stir welded joints prepared using the **a** CT and **b** BT
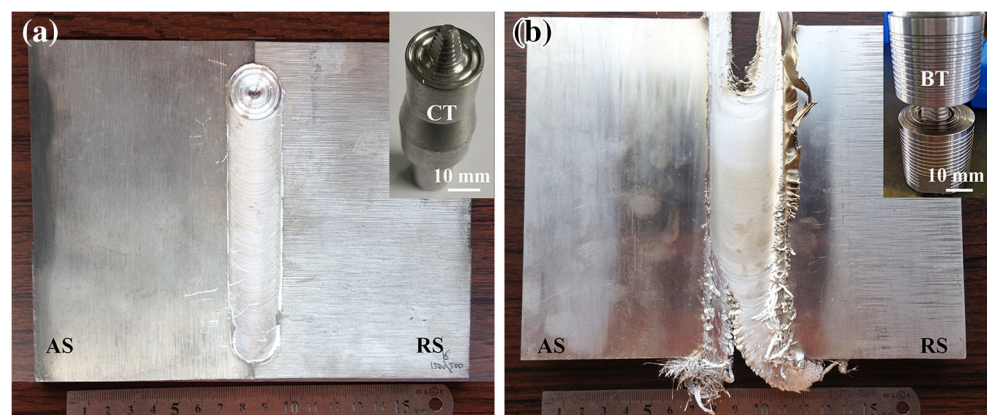
Generally, the friction stir welded AZ31 alloy joint is consisted of the BM, HAZ, TMAZ, and NZ due to the microstructure differences caused by different thermal cycle and plastic deformation. In addition, according to the difference between the rotation direction and forward direction of the tool, the two sides of the weld seam are defined as the advancing side (AS) and retreating side (RS), respectively. As a result, in addition to the HAZ, the TMAZ along the cross section of the joint is also divided into the AS and RS, respectively. Moreover, the HAZ and TMAZ on the AS and RS are labeled in abbreviated forms. For example, the HAZ on the AS is abbreviated as HAZ-AS. The low magnification OM microstructures of the various zones such as the NZ, TMAZ, HAZ, and BM in the friction stir welded joints prepared using the CT and BT are exhibited in Figs. 3 and 4, respectively. The BM consists of equiaxed grains having the mean grain size of 11.2 μm calculated according to the mean liner intercept method. The microstructures of the HAZ, TMAZ, and NZ in the joint prepared using the CT are also characterized by equiaxed grains, as shown in Fig. 3. The average grain sizes of the HAZ and TMAZ on the AS are 15.1 μm and 25.1 μm, respectively, while they are 12.2 μm and 16.9 μm on the RS. The average grain size of the NZ is 18.5 μm. Except that the grains in the TMAZ on the AS are slightly elongated, the microstructures of the other regions in the joint prepared using the BT are still characterized by equiaxed grains, as shown in Fig. 4. The average grain sizes of the HAZ and TMAZ on the AS are 20.6 μm and 11.3 μm, respectively, while they are 19.3 μm and 21.9 μm on the RS. The average grain size of the NZ is 18.9 μm. It can be found that the mean grain size in the various regions of the friction stir welded joints produced using the CT and BT is larger than that in the BM. Furthermore, a large difference in the mean grain size is observed between the HAZ-AS, TMAZ-AS, and NZ compared to that of the HAZ-RS, TMAZ-RS, and NZ.

For Mg-Al-Zn alloys, in addition to the average grain size, the distributions of the precipitates and dislocations also have a significant effect on the mechanical properties and corrosion performance. The distributions of the precipitates and dislocations of the as-received BM and NZ are shown in Figs. 5 and 6. The number of the $Al_{12}Mg_{17}$ precipitates in the NZ is more than that of the BM. Moreover, the distributions of the $Al_{12}Mg_{17}$ precipitates in the NZ are also more homogeneous than that in the BM, as shown in Fig. 5. In addition, some larger $Al_{12}Mg_{17}$ precipitates are observed in the NZ prepared using the BT compared to that of the CT, as shown in Figs. 5b and c. However, the size of the $Al_{12}Mg_{17}$ precipitate in the NZ prepared using the CT is similar to that of the BM, as shown in Figs. 5a and b. The distribution characteristics of the dislocations in the as-received BM and NZ prepared using the CT and BT exhibit that a large number of high-density dislocations and dislocation walls are promoted in the grains of the NZ compared to the BM, as shown in Fig. 6. In addition to the formation of a large number of fine recrystallized grains and subgrains, the high-density dislocations formed at the grain boundaries of the NZ prepared using the BT are also significantly more than that of the CT, as shown in Figs. 6b and c.

Previous studies have confirmed that the recrystallization temperature of magnesium alloy is about 205 °C [24]. Mironov et al. [25, 26] demonstrated that the welding temperature in the weld seam was increased from ~0.57 to ~0.85T_m with increasing the rotation speed from 300 to 2000 rpm during the FSW of a 4-mm thick AZ31 magnesium alloy plate, where T_m was the melting point of the AZ31 magnesium alloy. As a result, the peak temperature in the weld zone could easily reach the recrystallization temperature during FSW of
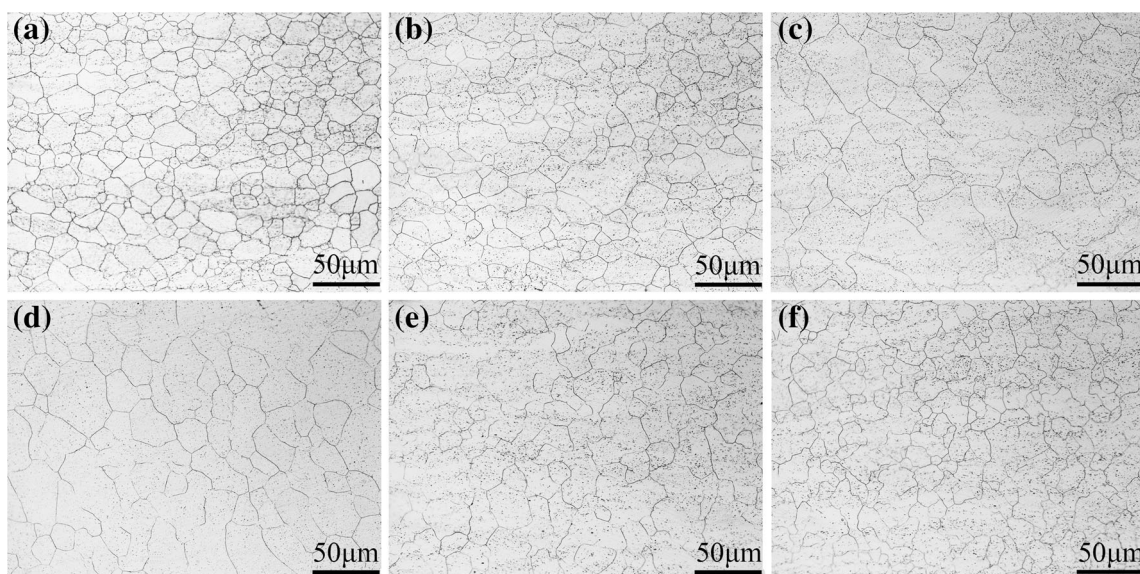
Fig. 3 Microstructures of the friction stir welded joint prepared using the CT **a** BM, **b** HAZ-AS, **c** TMAZ-AS, **d** NZ, **e** TMAZ-RS, and **f** HAZ-RS
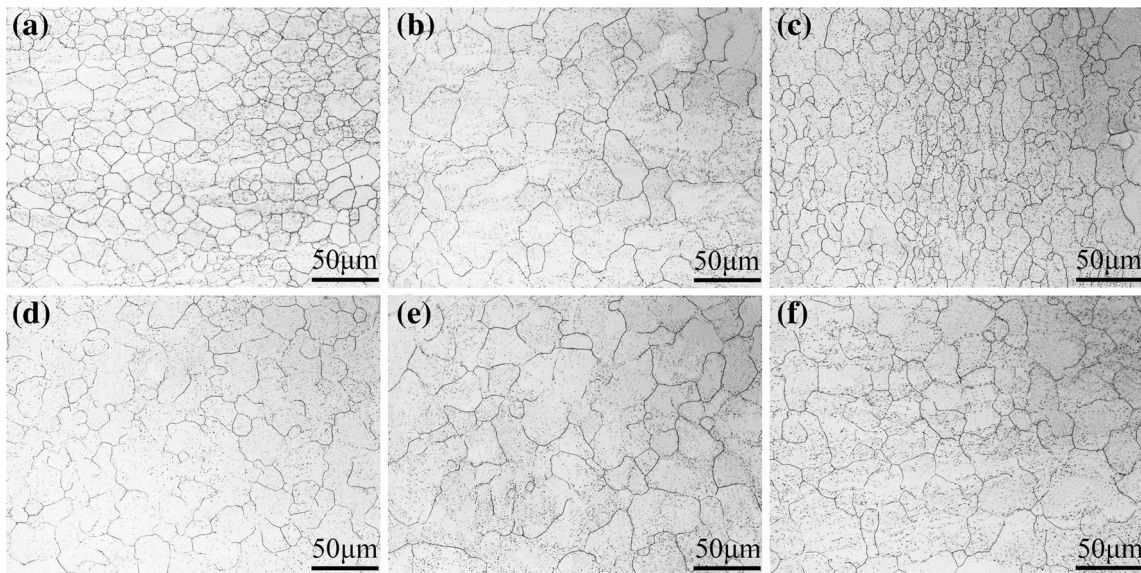
Fig. 4 Microstructures of the friction stir welded joint prepared using the BT **a** BM, **b** HAZ-AS, **c** TMAZ-AS, **d** NZ, **e** TMAZ-RS, and **f** HAZ-RS

magnesium alloy thick plates, and the dynamic recrystallization (DRX) occurred due to the high temperature and severe plastic deformation [27, 28]. In general, the complete DRX occurred in the NZ due to the most severe thermal cycle and plastic deformation. As a result, the equiaxed recrystallized grains in the NZ were significantly refined due to the complete DRX. In the TMAZ, incomplete DRX occurred due to the inadequate thermal cycle and plastic deformation compared to the NZ. Finally, the TMAZ had relatively larger recrystallized grains and deformed grains compared to the NZ. However, the HAZ only experienced thermal cycle, which eventually resulted in grain coarsening. Watanabe et al. [29] developed a model using the BM grain size (D_{BM}) and Zener-Hollomon parameter (Z) for calculating grain size of the NZ (D_{NZ}) varied from to 100 μm.

$$\frac{D_{NZ}}{D_{BM}} = 10^3 Z^{-1/3} \tag{1}$$

The Z can be calculated using the strain rate ($\dot{\varepsilon}$), the NZ temperature (T), and the activation energy (Q) for lattice diffusion and the gas constant (R) [30].

$$Z = \dot{\varepsilon}\exp(Q/RT) \tag{2}$$

According to the Eqs. (1) and (2), it could be known that the welding temperature and strain rate became the main factors affecting the grain size for a constant BM. Increasing the strain rate and decreasing the welding temperature could refine the grain size in the NZ.

In the present work, in addition to undergoing the strong plastic deformation, the NZ also experienced severe thermal cycle, which resulted in a long high temperature residence times in the cooling stage. As a result, the recrystallized grains in the NZ were significantly coarsened. Due to the absence of heat dissipation between the workpiece and backing plate by heat conduction, the NZ prepared using the BT experienced a longer high temperature residence times compared to the CT,
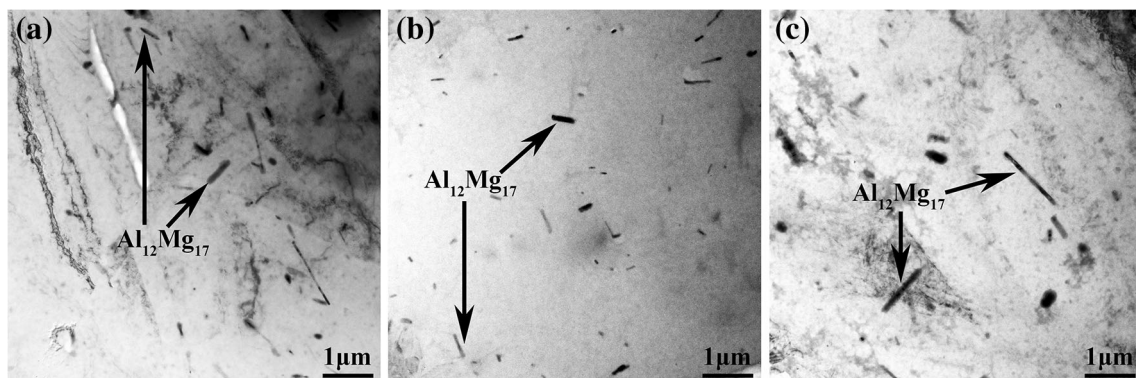
Fig. 5 Distribution characteristics of precipitate in the **a** BM and NZ prepared using the **b** CT and **c** BT
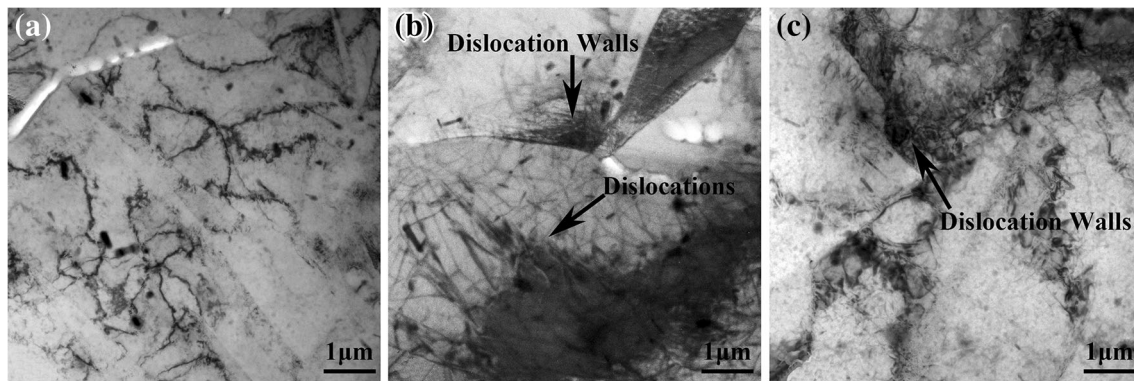
**Fig. 6** Microstructure characteristics of the **a** BM and NZ prepared using the **b** CT and **c** BT

which further resulted in a larger grain size, as shown in Figs. 3d and 4d. It is also well known that, in addition to accelerating the rapid initiation and propagation of dislocations, the severe plastic deformation and high welding temperature also contribute to enhance more supersaturated and metastable solid solutions in the weld zone. In the subsequent cooling stage, a large number of high-density dislocations, dislocation walls, and $Al_{12}Mg_{17}$ precipitates are formed in the NZ. At longer high temperature residence times, compared with the CT, more dislocation walls and larger $Al_{12}Mg_{17}$ precipitates are formed in the NZ prepared using the BT due to the strengthening of dislocation motion and severe growth of the $Al_{12}Mg_{17}$ precipitates, as shown in Figs. 5c and 6c. In the TMAZ and HAZ, the welding temperature on the AS is higher than that on the RS during FSW. As a result, the grain sizes in the TMAZ-AS and HAZ-AS prepared using the CT are larger than those of the TMAZ-RS and HAZ-RS, as shown in Fig. 3. However, the grain size in the TMAZ-AS prepared using the BT is smaller than that of the TMAZ-RS, which is probably due to the main role of the strain rate, as shown in Figs. 4c and e. The grain size in the HAZ-AS prepared using the BT is larger than that of the HAZ-RS due to higher heat input, as shown in Figs. 4b and f. In addition, the peak temperature difference between the TMAZ and HAZ during FSW with the CT is greater than that of the BT. Therefore, a large difference in grain size between the TMAZ and HAZ prepared using the CT is produced. There is also a large difference in grain size between the TMAZ-AS and NZ due to the difference in the peak temperature and strain rate.

3.2 Microhardness

Figure 7 shows the microhardness distributions along the mid-thickness of the friction stir welded joints prepared using the CT and BT. Compared with the BM, a very slight variation in microhardness value of the joints is observed. These phenomena are similar to the previous microhardness test results in friction stir welded AZ31 alloy joints produced using the CT

[31] and BT [32]. The microhardness values vary between 54 HV and 59 HV. The microhardness distribution exhibits a relatively obvious discontinuity between the NZ and TMAZ-AS. The mean microhardness value in the NZ of the joint prepared using the BT is larger than that of the CT. In this study, it can be seen that the influence of grain size on microhardness does not follow the Hall-Petch equation.

It is well known that the changes in microhardness values are mainly related to the grain size, dislocation density, and precipitate or intermetallic compound distribution. The BM used in the present work is not precipitation-strengthened non-ferrous metal material. Therefore, the changes in dissolution and reprecipitation of the $Al_{12}Mg_{17}$ during FSW do not play a substantial role in the microhardness value. The microhardness value in the FSW of AZ31 alloy depends on the grain size and dislocation. According to the Hall-Petch relationship, the microhardness values in the friction stir welded joints should be smaller than that in the BM due to the larger grains, but the microhardness values in the joints and BM are basically identical. The slight change in the microhardness value of the joint
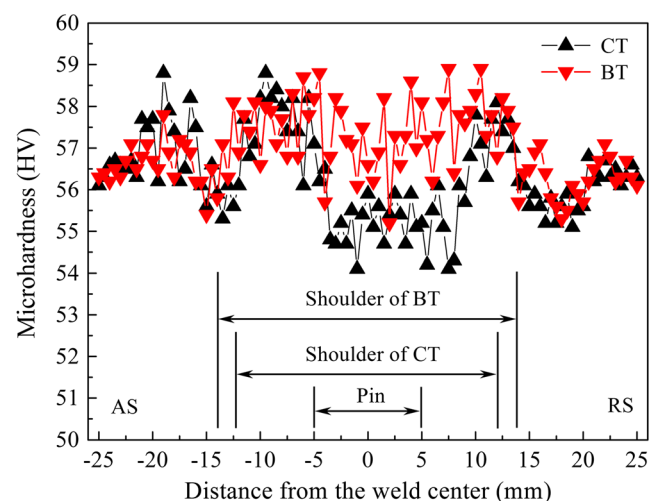

Fig. 7 Microhardness distributions of the friction stir welded joints prepared using the CT and BT

is probably related to the change of the dislocation density and residual stress. Esparza et al. [33] found that a slight increase in the microhardness value of the NZ during FSW of a 6.4-mm thick AZ31 alloy plate is attributed to relatively high-density dislocations and residual stresses. In this study, more high-density dislocations in the NZ of the friction stir welded joint prepared using the BT are produced compared to that of the CT. As a result, a relatively high microhardness value is exhibited in the NZ of the joint prepared using the BT, as shown in Fig. 7.

3.3 Tensile properties

Figure 8 illustrates the tensile test results of the BM and friction stir welded joints produced by the CT and BT. The ultimate tensile strength (UTS), yield strength (YS), and elongation (EL) extracted from the stress-strain curves of the BM and joints are also exhibited in Fig. 8. It is clear that the tensile properties of all friction stir welded joints are inferior to the BM. This is consistent with the results in FSW of AZ31 alloy carried out by Commin et al. [31] and Li et al. [32], who also found a reduction in tensile properties. The UTS, YS, and EL of the joint prepared using the CT reach 85.3%, 49.1%, and 72.0% of those of the BM, respectively, whereas 83.5%, 61.6%, and 89.9% in the joint prepared using the BT. Compared with the CT, the joint prepared by the BT exhibits more excellent tensile properties.

The explanations about the tensile strength degradation of the friction stir welded AZ31 alloy joints mainly focus on the following aspects. Firstly, the UTS and YS are related to the microhardness value of the joint. In fact, low microhardness value region in the joint always exists in the transition regions of TMAZ/NZ [24, 32, 33]. It is easy to form stress concentration in the low microhardness region during tensile test, which further leads to crack initiation and propagation in this region.
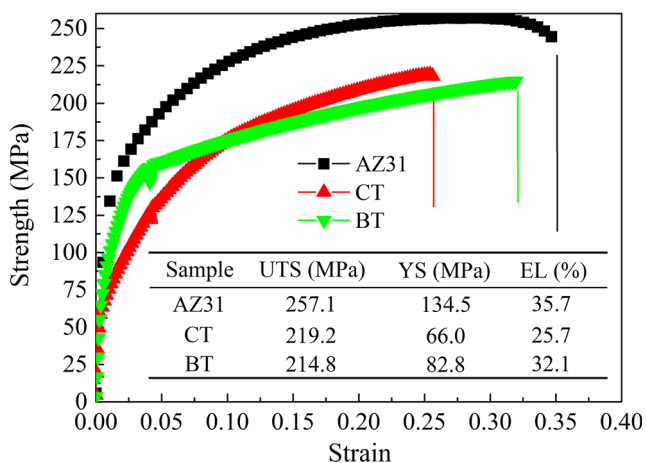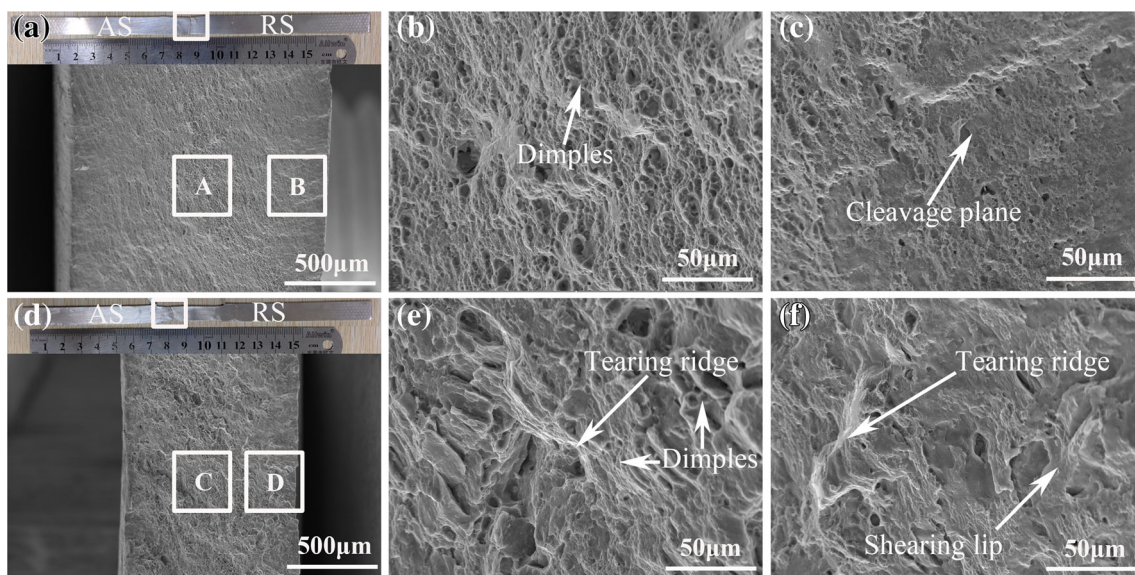
Secondly, different crystal orientation exists in the various regions of the joint due to the difference in the thermal cycle and plastic deformation [34]. In the process of tensile test, incompatible deformation occurs in the adjacent regions of the joint due to different crystal orientation in favor of different deformation mechanism. As a result, the fracture occurs in this region. Thirdly, dislocation density and residual stress in the various regions of the joint have an obvious effect on the joint strength [33]. The low dislocation density cannot effectively prevent the dislocation movement during tensile test, and it is easy to preferentially form localized plastic deformation and crack in this region. In addition, the residual tensile stress in the joint can reduce the total tensile stress, resulting in a reduction in the joint strength. In this study, a low microhardness value and obvious microstructure difference in the transition region of the TMAZ-AS/NZ are exhibited, which induces the friction stir welded AZ31 alloy thick plate joint to fracture in this region during tensile test, as shown in Figs. 9a and d. In addition to the formation of a large number of high-density dislocations and dislocation walls in the NZ, a relatively more homogeneous microstructure of the joint prepared by the BT is exhibited compared to the CT. As a result, the joint prepared by the BT exhibits higher YS and EL than those of the CT.

Figure 9 presents details of the fracture locations and fracture surfaces of the friction stir welded AZ31 alloy thick plate joints after tensile test. Three different zones on the fracture surface of the joints presenting brittle and ductile fracture features were observed, as shown in Figs. 9a and d. The brittle fracture occurs on the surface of both sides of the joint, where characterizes by a large number of cleavage planes and shearing lips, as shown in Figs. 9c and f. The ductile fracture occurs in the center of the joint fracture surface, where characterizes by a large number of shallow dimples at the CT and large tearing ridges at the BT, as shown in Figs. 9b and e. Furthermore, compared with the BT, the fracture surface of the joint prepared by the CT is flatter. This is consistent with the tensile test results, of which the EL is smaller than that of the BT.
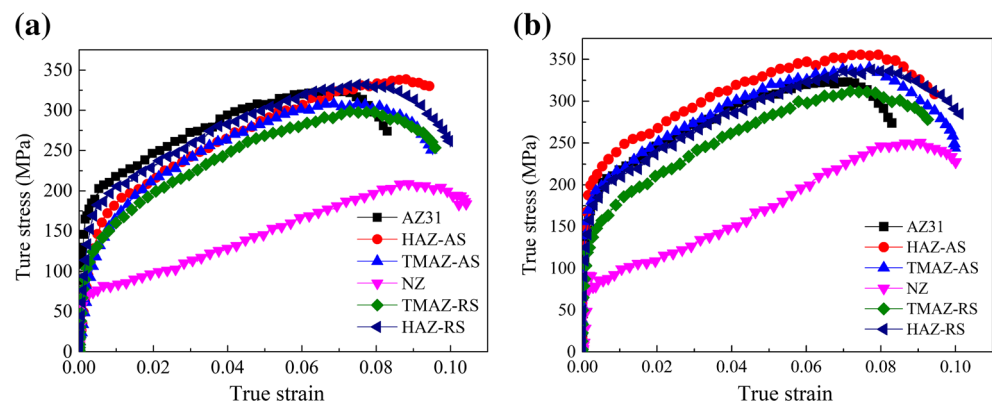
3.4 Dynamic compressive mechanical properties

Figure 10 indicates the typical compressive stress-strain curves of the BM, and various regions in the friction stir welded joints produced by the CT and BT and the corresponding YS, ultimate compressive strength (UCS), and compressive fraction elongation (CFE) are summarized in Table 1. The YS, UCS, and CTE of the as-received BM are 180.7 MPa, 326.5 MPa, and 8.3%, respectively. Compared with the BM, in addition to a slight fluctuation in the UCS, the YS of the various regions in the joint, especially in the NZ, is reduced to a certain extent. However, the various regions in the joint exhibit better CFE than that of the BM. In addition, the YS and UCS of the various regions in the joint prepared by the BT are better than those of the CT.

Sample	UTS (MPa)	YS (MPa)	EL (%)
AZ31	257.1	134.5	35.7
CT	219.2	66.0	25.7
BT	214.8	82.8	32.1

Fig. 8 Tensile properties of the BM and friction stir welded joints prepared using the CT and BT

Fig. 9 Fracture location and fractography of the friction stir welded joints prepared using the **a-c** CT and **d-f** BT, and magnified morphologies of areas **b** A, **c** B, **e** C, and **f** D

Fig. 10 Dynamic properties of the friction stir welded joints prepared using the **a** CT and **b** BT

It is well known that the main factors affecting the dynamic compressive mechanical properties of magnesium alloy can be attributed to the following aspects. Firstly, the dynamic compressive mechanical properties are related to the basal texture. The basal slip and {10–12} extension twins with low critical shear stress are the most important plastic deformation mechanism during compression test [35, 36]. The {10–12} extension twinning can easily result in the activation of pyramidal slip or contraction twins during high strain rate compression test, which requires high stress [37]. Secondly, the dislocation density, subgrain, and precipitate characteristic have a significant influence on the dynamic

Table 1 Dynamic compressive mechanical properties of the BM and various regions of the friction stir welded joints

Samples	CT			BT		
	YS (MPa)	UCS (MPa)	CFE (%)	YS (MPa)	UCS (MPa)	CFE (%)
HAZ-AS	178.3	338.4	9.3	205.6	357.9	9.5
TMAZ-AS	141.2	308.6	9.5	177.2	340.4	10.0
NZ	71.2	209.5	10.3	81.3	251.3	10.1
TMAZ-RS	122.5	299.8	9.6	129.5	314.3	9.3
HAZ-RS	169.6	328.6	10.0	176.5	338.4	10.2

compressive mechanical properties. The high-density dislocations, subgrain boundaries, and precipitates in the grain boundaries inhibit the dislocation movement and nucleation and growth of adjacent grains during compression test, which play a role in pinning strength [38]. As a result, the dynamic compressive mechanical properties are enhanced. Thirdly, the grain size has an effect on the dynamic compressive mechanical properties. According to the Hall-Petch law, the yield stress (σ_{YS}) can be calculated by the grain size (d) [39].

$$\sigma_{YS} = \sigma_0 + kd^{-1/2} \tag{3}$$

where σ_0 is the material constant, and k is the slope.

It is evident from the Eq. (3) that the fine grain size can effectively improve the strength. It is also found that the decrease in grain size can increase the critical shear stress for activating {10–12} extension twins [39]. In this study, the mean grain size and basal texture in the BM are finer and stronger than those in the various regions of the joints, resulting in excellent dynamic compressive mechanical properties. Previous results in the FSW of magnesium alloys have demonstrated that different crystal orientation exists in the various regions of the joint due to the difference in the plastic deformation and thermal cycle [34]. In addition to the dislocation density, the number and distribution of the precipitates are larger and more homogeneous in the various regions of the joint prepared by the BT than those of the CT, which further resulting in better dynamic compressive mechanical properties. However, in addition to the difference of the crystal orientation, the differences of the dislocation density, precipitates, and grain sizes in the various regions of the joint result in a various dynamic compressive mechanical properties, as shown in Fig. 10.

3.5 Corrosion resistance

Figure 11 illustrates the potentiodynamic polarization curves of the BM and various regions of the friction stir welded joints

produced using the CT and BT in a 3.5 wt% NaCl solution. The corresponding self-corrosion potential and self-corrosion current calculated using the Tafel extrapolation method are summarized in Table 2. The self-corrosion potential and self-corrosion current of the BM are −1.49 V and 1.83 × 10^{-4} A, respectively. Compared with the BM, the various regions in the joints exhibit excellent corrosion resistance, especially in the joint prepared by the BT. The self-corrosion potential increases from −1.49 to −1.37 V, whereas the self-corrosion current decreases from 1.83 × 10^{-4} to 4.86 × 10^{-5} A.

Figure 12 shows the Nyquist spectras of the BM and various regions of the friction stir welded joints produced by the CT and BT. It can be seen from the Nyquist spectras that the diameters of the capacitive loops in the various regions of the joints are obviously larger than that of the BM. In addition, the diameters of the capacitive loops in the various regions of the joint produced by the BT are significantly larger than that of the CT. The Nyquist spectras also ascertain that the various regions of the joints prepared by the CT and BT, especially by the BT, have a better corrosion resistance than that of the BM.

Figure 13 presents the corrosion attack morphologies of the BM and various regions of the friction stir welded joint produced by the BT after corrosion test. The corrosion pits on the corrosion attack surface of the BM are large and deep, which indicate that the BM has suffered severe corrosion attack, as shown in Fig. 13a. Relatively small and shallow corrosion pits are observed on the surface of the HAZ-AS and HAZ-RS, indicating that the corrosion attack in these regions is less than that in the BM, as shown in Figs. 13b and f. In the TMAZ-AS and TMAZ-RS, some small and shallow corrosion pits are widely distributed on the corrosion surface, which indicates that a relatively homogeneous corrosion attack has been experienced in these regions, as shown in Figs. 13c and e. However, in the NZ, the corrosion pits observed on the corrosion surface are larger and deeper than that in the TMAZ, but smaller and shallower than that in the HAZ, as shown in Fig. 13d. It can be inferred that

Fig. 11 Potentiodynamic polarization curves of the BM and friction stir welded joints prepared using the a CT and b BT
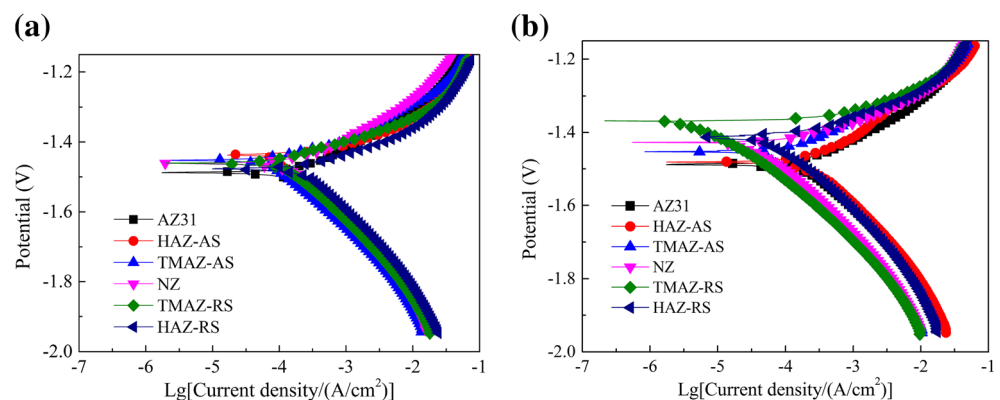
Table 2 Electrochemical parameters of potentiodynamic polarization curves of the BM and friction stir welded joints calculated by the Tafel extrapolation method

Samples	Self-corrosion potential (V)					Self-corrosion current (A)				
	HAZ-AS	TMAZ-AS	NZ	TMAZ-RS	HAZ-RS	HAZ-AS	TMAZ-AS	NZ	TMAZ-RS	HAZ-RS
CT	−1.44	−1.45	−1.46	−1.48	−1.46	2.82×10^{-4}	1.26×10^{-4}	1.70×10^{-4}	1.51×10^{-4}	1.56×10^{-4}
BT	−1.48	−1.45	−1.43	−1.37	−1.41	2.37×10^{-4}	5.73×10^{-5}	8.75×10^{-5}	4.86×10^{-5}	1.10×10^{-4}

Fig. 12 Nyquist spectras of the BM and friction stir welded joints prepared using the **a** CT and **b** BT
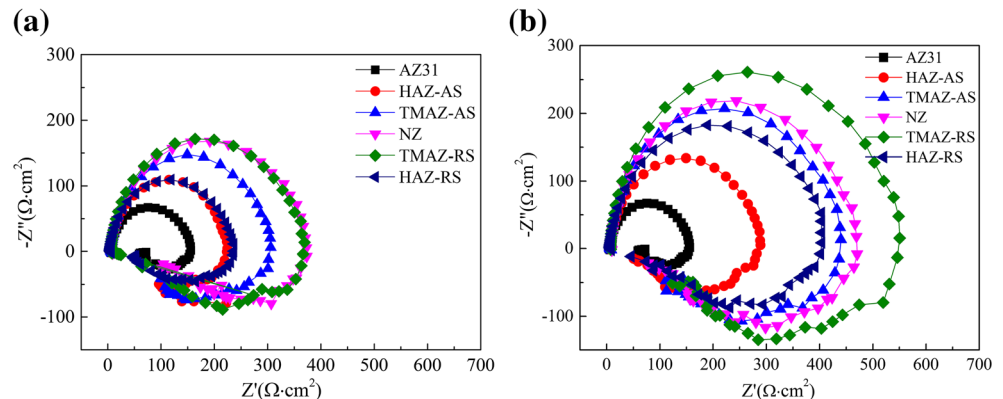
the corrosion attack in the NZ is more severe than that in the TMAZ, but less than that in the HAZ.

It is well known that the corrosion resistance of the Mg-Al-Zn alloy is mainly affected by grain size and precipitate characteristics according to the previous research results [40–42]. Seifiyan et al. [40] found that the friction stir processed AZ31 alloy exhibited excellent corrosion resistance due to the formation of fine grain structure. Liu et al. [41] demonstrated that plentiful grain boundaries could enhance the corrosion resistance of ultrafine-grained AZ31 alloy prepared by severe shot peening due to the rapid formation of a relatively compact and stable passive film. However, Liu et al. [42] reported that the
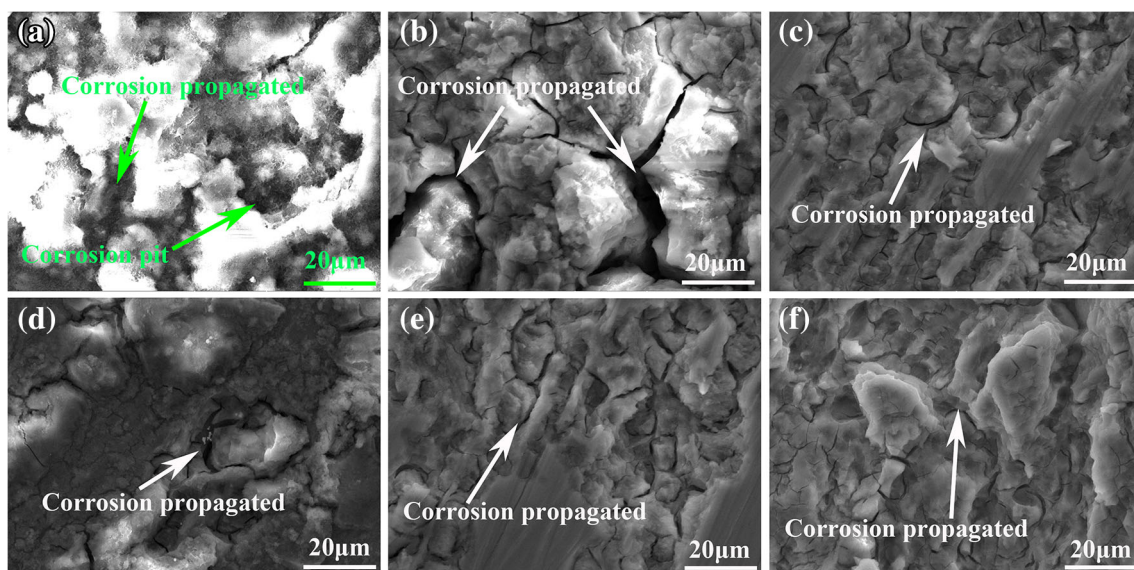
Fig. 13 Corrosion morphology on the surface of the **a** BM, **b** HAZ-AS, **c** TMAZ-AS, **d** NZ, **e** TMAZ-RS, and **f** HAZ-RS prepared using the BT

size and distribution of the precipitates are the main factors affecting the corrosion resistance of the Mg-Al-Zn alloys. The precipitates mainly improve the corrosion resistance of Mg-Al-Zn alloys by altering the galvanic corrosion between α-Mg/precipitate. In this study, although the mean grain sizes in the various regions of the joints are larger than that in the BM, the corrosion resistances of these various regions are better than that of the BM. It can be inferred that the main factor affecting the corrosion resistance of the friction stir welded AZ31 alloy thick plate joint is not the mean grain size but the size and distribution of the $Al_{12}Mg_{17}$ precipitate. The sizes and distributions of the $Al_{12}Mg_{17}$ precipitates in the NZ prepared by the BT are larger and more uniform than those of the CT, which result in better corrosion resistance in this region. In addition to forming uniform distributions, the sizes of the $Al_{12}Mg_{17}$ precipitates in the TMAZ are likely to be smaller than those in the NZ, which is mainly due to the inadequate plastic deformation and thermal cycling. As a result, the TMAZ exhibits better corrosion resistance than that of the NZ. In the HAZ, some $Al_{12}Mg_{17}$ precipitates are coarsened to some extent due to the thermal cycle, resulting in poor corrosion performance in this region. In addition, because the thermal cycle and plastic deformation along the plate thickness direction of the various regions in the friction stir welded joints prepared by the BT are significantly more uniform than those of the CT, the sizes and distributions of the $Al_{12}Mg_{17}$ precipitates in these regions are also more uniform than those of the CT. As a result, the various regions in the friction stir welded joint prepared by the BT exhibit better corrosion resistance than those of the CT.

4 Conclusions

(1) Sound friction stir welded AZ31 alloy thick plate joints without any defects were produced using both CT and BT. A large number of $Al_{12}Mg_{17}$ precipitates and high-density dislocations in the NZ were obtained. A relatively more homogeneous microstructure between the adjacent regions of the joint prepared by the BT was observed compared with the CT.

(2) The friction stir welded AZ31 alloy thick plate joint produced using the BT exhibited excellent tensile properties and dynamic compressive mechanical properties due to a relatively more homogeneous microstructure and a larger number of precipitates and high density dislocations compared with the CT. The joint efficiency reached 83.5~85.3% of the BM, whereas all the joints presented significantly lower YS than that of the BM. All the joints fractured in the transition region of the TMAZ-AS/NZ.

(3) The corrosion resistance of the various regions in the friction stir welded joint produced by the BT was significantly enhanced compared to the BM. The self-corrosion potential increased from -1.49 to -1.37 V, whereas the self-corrosion current decreased from 1.83×10^{-4} to 4.86×10^{-5} A. The main factor affecting the corrosion resistance of the joint was the sizes and distributions of the precipitates rather than the mean grain size.

(4) FSW with BT was considered to be the most effective method for welding AZ31 alloy thick plate due to formation of the relatively homogeneous microstructure and excellent mechanical and corrosion resistance properties.

References

1. Xiong XM, Yang Y, Li JG, Li MM, Peng J, Wen C, Peng XD (2019) Research on the microstructure and properties of a multi-pass friction stir processed 6061Al coating for AZ31 Mg alloy. J Magnes Alloys 7(4):696–706. https://doi.org/10.1016/j.jma.2019.09.001

2. Rezaei M, Jabbari AH, Sedighi M (2020) Investigation of surface roughness effects on microstructural and mechanical properties of diffusion bonding between dissimilar AZ91-D magnesium and AA6061 aluminum alloys. Weld World 64:949–962. https://doi.org/10.1007/s40194-020-00883-6

3. Ogura T, Yokochi T, Netsu S, Saida K (2016) Microstructure and mechanical properties in laser brazing of A5052/AZ31 dissimilar alloys. Weld World 60:1047–1054. https://doi.org/10.1007/s40194-016-0363-3

4. Carlone P, Palazzo GS (2015) Characterization of TIG and FSW weldings in cast ZE41A magnesium alloy. J Mater Process Technol 215:87–94. https://doi.org/10.1016/j.jmatprotec.2014.07.026

5. Liu HT, Zhou JX, Zhao DQ, Liu YT, Wu JH, Yang YS, Ma BC, Zhuang HH (2017) Characteristics of AZ31 Mg alloy joint using automatic TIG welding. Int J Miner Metall Mater 24(1):102–108. https://doi.org/10.1007/s12613-017-1383-8

6. Liu XC, Sun YF, Nagira T, Ushioda K, Fujii H (2019) Experimental evaluation of strain and strain rate during rapid cooling friction stir welding of pure copper. Sci Technol Weld Join 24(7):352–359. https://doi.org/10.1080/13621718.2018.1556436

7. Zhou L, Zhang RX, Hu XY, Guo N, Zhao HH, Huang YX (2019) Effects of rotation speed of assisted shoulder on microstructure and mechanical properties of 6061-T6 aluminum alloy by dual-rotation friction stir welding. Int J Adv Manuf Technol 100:199–208. https://doi.org/10.1007/s00170-018-2570-0

8. Singh K, Singh G, Singh H (2018) Review on friction stir welding of magnesium alloys. J Magnes Alloys 6(4):399–416. https://doi.org/10.1016/j.jma.2018.06.001

9. Templeman Y, Hamu GB, Meshi L (2017) Friction stir welded AM50 and AZ31 Mg alloys: microstructural evolution and improved corrosion resistance. Mater Charact 126:86–95. https://doi.org/10.1016/j.matchar.2017.02.018

10. Singh K, Singh G, Singh H (2018) Investigation of microstructure and mechanical properties of friction stir welded AZ61 magnesium alloy joint. J Magnes Alloys 6(3):292–298. https://doi.org/10.1016/j.jma.2018.05.004

11. Shang Q, Ni DR, Xue P, Xiao BL, Ma ZY (2017) Evolution of local texture and its effect on mechanical properties and fracture behavior of friction stir welded joint of extruded Mg-3Al-1Zn alloy. Mater Charact 128:14–22. https://doi.org/10.1016/j.matchar.2017.03.018

12. Mironov S, Onuma T, Sato YS, Yoneyama S, Kokaw H (2017) Tensile behavior of friction-stir welded AZ31 magnesium alloy. Mater Sci Eng A 679:272–281. https://doi.org/10.1016/j.msea.2016.10.036

13. Zeng RC, Chen J, Dietzel W, Zettler R, Santos JFD, Nascimento ML, Kainer KU (2009) Corrosion of friction stir welded magnesium alloy AM50. Corros Sci 51(8):1738–1746. https://doi.org/10.1016/j.corsci.2009.04.031

14. Suhuddin UFHR, Mironov S, Sato YS, Kokawa H, Lee CW (2009) Grain structure evolution during friction-stir welding of AZ31 magnesium alloy. Acta Mater 57(18):5406–5418. https://doi.org/10.1016/j.actamat.2009.07.041

15. Chowdhury SH, Chen DL, Bhole SD, Cao X, Wanjara P (2013) Friction stir welded AZ31 magnesium alloy: microstructure, texture, and tensile properties. Metall Mater Trans A 44:323–336. https://doi.org/10.1007/s11661-012-1382-3

16. Wang WD, Deng DA, Mao ZT, Tong YG, Ran Y (2017) Influence of tool rotation rates on temperature profiles and mechanical properties of friction stir welded AZ31 magnesium alloy. Int J Adv Manuf Technol 88:2191–2200. https://doi.org/10.1007/s00170-016-8918-4

17. Ugender S (2018) Influence of tool pin profile and rotational speed on the formation of friction stir welding zone in AZ31 magnesium alloy. J Magnes Alloys 6(2):205–213. https://doi.org/10.1016/j.jma.2018.05.001

18. Liu G, Ma LN, Ma ZD, Fu XS, Wei GB, Yang Y, Xu TC, Xie WD, Peng XD (2018) Effects of welding speed and post-weld hot rolling on microstructure and mechanical properties of friction stir-welded AZ31 magnesium alloy. Acta Metall Sin (Engl Lett) 31:853–864. https://doi.org/10.1007/s40195-018-0725-5

19. Darras B, Emad K (2013) Submerged friction stir processing of AZ31 magnesium alloy. Mater Des 47:133–137. https://doi.org/10.1016/j.matdes.2012.12.026

20. Rouhi S, Mostafapour A, Ashjari M (2016) Effects of welding environment on microstructure and mechanical properties of friction stir welded AZ91C magnesium alloy joints. Sci Technol Weld Join 21(1):25–31. https://doi.org/10.1179/1362171815Y.0000000058

21. Shen CB (2013) Corrosion characteristics of friction stir welded AZ31 magnesium alloy. Adv Mater Res 785-786:97–100. https://doi.org/10.4028/www.scientific.net/AMR.785-786.97

22. Abbasi M, Abdollahzadeh A, Omidvar H, Bagheri B, Rezaei M (2016) Incorporation of SiC particles in FS welded zone of AZ31 Mg alloy to improve the mechanical properties and corrosion resistance. Int J Mater Res 107(6):1–7. https://doi.org/10.3139/146.111369

23. Sahu PK, Vasudevan NP, Das B, Pal S (2019) Assessment of self-reacting bobbin tool friction stir welding for joining AZ31 magnesium alloy at inert gas environment. J Magnes Alloys 7(4):661–671. https://doi.org/10.1016/j.jma.2019.05.011

24. Li WY, Niu PL, Yan SR, Patel V, Wen Q (2019) Improving microstructural and tensile properties of AZ31B magnesium alloy joints by stationary shoulder friction stir welding. J Manuf Process 37:159–167. https://doi.org/10.1016/j.jmapro.2018.11.014

25. Mironov S, Onuma T, Sato YS, Kokawa H (2015) Microstructure evolution during friction-stir welding of AZ31 magnesium alloy. Acta Mater 100:301–312. https://doi.org/10.1016/j.actamat.2015.08.066

26. Mironov S, Sato YS, Kokawa H (2019) Influence of welding temperature on material flow during friction stir welding of AZ31 magnesium alloy. Metall Mater Trans A 50:2798–2806. https://doi.org/10.1007/s11661-019-05194-0

27. Liu XC, Sun YF, Nagira T, Ushioda K, Fujii H (2019) Evaluation of dynamic development of grain structure during friction stir welding of pure copper using a quasi in situ method. J Mater Sci Technol 35:1412–1421. https://doi.org/10.1016/j.jmst.2019.01.018

28. Zhang JL, Liu K, Huang GS, Chen X, Xia DB, Jiang B, Tang AT, Pan FS (2020) Optimizing the mechanical properties of friction stir welded dissimilar joint of AM60 and AZ31 alloys by controlling deformation behavior. Mater Sci Eng A 773:138839. https://doi.org/10.1016/j.msea.2019.138839

29. Watanabe H, Tsutsui H, Mukai T, Ishikawa H, Okanda Y, Kohzu M, Higashi K (2001) Grain size control of commercial wrought Mg-Al-Zn alloys utilizing dynamic recrystallization. Mater Trans 42(7):1200–1205. https://doi.org/10.2320/matertrans.42.1200

30. Chang CI, Lee CJ, Huang JC (2004) Relationship between grain size and Zener–Holloman parameter during friction stir processing in AZ31 Mg alloys. Scr Mater 51(6):509–514. https://doi.org/10.1016/j.scriptamat.2004.05.043

31. Commin L, Dumont M, Masse JE, Barrallier L (2009) Friction stir welding of AZ31 magnesium alloy rolled sheets: influence of processing parameters. Acta Mater 57(2):326–334. https://doi.org/10.1016/j.actamat.2008.09.011

32. Li WY, Fu T, Hütsch L, Hilgert J, Wang FF, Dos Santos JF, Huber N (2014) Effects of tool rotational and welding speed on microstructure and mechanical properties of bobbin-tool friction-stir welded Mg AZ31. Mater Des 64:714–720. https://doi.org/10.1016/j.matdes.2014.07.023

33. Esparza JA, Davis WC, Trillo EA, Murr LE (2002) Friction-stir welding of magnesium alloy AZ31B. J Mater Sci Lett 21:917–920. https://doi.org/10.1023/A:1016061303955

34. Li GH, Zhou L, Luo SF, Dong FB, Guo N (2020) Microstructure and mechanical properties of bobbin tool friction stir welded ZK60 magnesium alloy. Mater Sci Eng A 776:138953. https://doi.org/10.1016/j.msea.2020.138953

35. Wang RF, Mao PL, Liu YY, Chen Y, Wang Z, Wang F, Zhou L, Liu Z (2019) Influence of pre-twinning on high strain rate compressive behavior of AZ31 Mg-alloys. Mater Sci Eng A 742:309–317. https://doi.org/10.1016/j.msea.2018.09.055

36. Knezevic M, Levinson A, Harris R, Mishra RK, Doherty RD, Kalidindi SR (2010) Deformation twinning in AZ31: influence on strain hardening and texture evolution. Acta Mater 58:6230–6242. https://doi.org/10.1016/j.actamat.2010.07.041

37. Hong SG, Park SH, Chong SL (2011) Strain path dependence of {10-12} twinning activity in a polycrystalline magnesium alloy. Scr Mater 64(2):145–148. https://doi.org/10.1016/j.scriptamat.2010.09.030

38. Kumar A, Wang J, Tomé CN (2015) First-principles study of energy and atomic solubility of twinning-associated boundaries in hexagonal metals. Acta Mater 85:144–154. https://doi.org/10.1016/j.actamat.2014.11.015

39. Chen Y, Tekumalla S, Guo YB, Shabadi R, Shim VPW, Gupta M (2017) The dynamic compressive response of a high-strength magnesium alloy and its nanocomposite. Mater Sci Eng A 702:65–72. https://doi.org/10.1016/j.msea.2017.07.005

40. Seifiyan H, Sohi MH, Ansari M, Ahmadkhaniha D, Saremi M (2019) Influence of friction stir processing conditions on corrosion behavior of AZ31B magnesium alloy. J Magnes Alloys 7(4):605–616. https://doi.org/10.1016/j.jma.2019.11.004

41. Liu CC, Zheng H, Gu X, Jiang BL, Liang J (2019) Effect of severe shot peening on corrosion behavior of AZ31 and AZ91 magnesium alloys. J Alloys Compd 770:500–506. https://doi.org/10.1016/j.jallcom.2018.08.141

42. Liu M, Uggowitzer PJ, Nagasekhar AV, Schmutz P, Easton M, Song GL (2009) Calculated phase diagrams and the corrosion of die-cast Mg–Al alloys. Corros Sci 51(3):602–619. https://doi.org/10.1016/j.corsci.2008.12.015